

One-Shot Radiance: Global Illumination Using Convolutional Autoencoders

Giulio Jiang¹ and Bernhard Kainz¹

¹Imperial College London

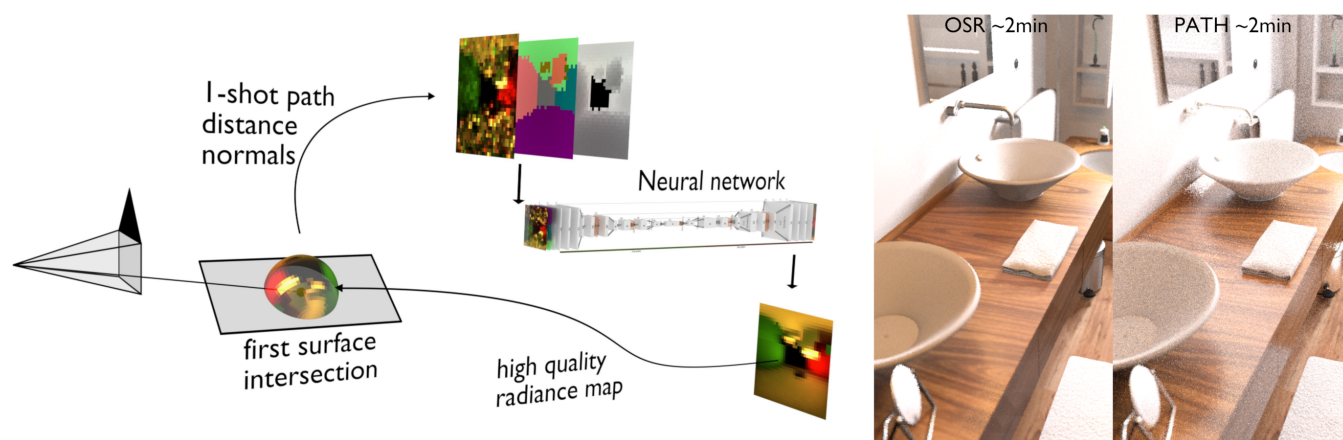


Figure 1: Our proposed One-Shot Radiance (OSR) method evaluates a low quality radiance map rendered at 1 sample per pixel (one-shot), distance and normal map at the first intersection, and uses a neural network to obtain a higher quality radiance map containing an accurate approximation of all indirect lighting. The Bathroom scene in this image from PBRTv3’s scenes [PJH18] shows OSR compared to a same-time path traced image. OSR produces a noise-free result with convincing global illumination after 30 seconds (1xCPU), and progressively refines quality afterwards.

Abstract

Rendering realistic images with Global Illumination (GI) is a computationally demanding task and often requires dedicated hardware for feasible runtime. Recent projects have used Generative Adversarial Networks (GAN) to predict indirect lighting on an image level, but are limited to diffuse materials and require training on each scene. We present One-Shot Radiance (OSR), a novel machine learning technique for rendering Global Illumination using Convolutional Autoencoders. We combine a modern denoising Neural Network with Radiance Caching to offer high performance CPU GI rendering while supporting a wide range of material types, without the requirement of offline pre-computation or training for each scene. OSR has been evaluated on interior scenes, and is able to produce high-quality images within 180 seconds on a single CPU.

CCS Concepts

•Computing methodologies → Ray tracing; Neural networks;

1. Introduction

Ray Tracing is capable of producing photo-realistic images virtually indistinguishable from real pictures. Progressive refinements on rendering algorithms, such as Bi-Directional Path tracing [LW93] and Metropolis Light Transport [VG97] have increased the efficiency of rendering engines in scenarios in which light paths are difficult to evaluate due to the high amount of indirect light-

ing and Global Illumination (GI). Complex lighting conditions are however still highly expensive to resolve, and most algorithms require long rendering times to reduce the noise from Monte Carlo sampling.

Biased methods have been implemented to produce convincing quality images at a fraction of the cost required by a ray tracer. An early method, Instant Radiosity [Kel97], exploited the low rate

of illumination change over diffuse surfaces to approximate GI by rendering the same scene many times using Virtual Point Lights sampled at locations reached by the main light sources to simulate secondary bounces.

Radiance Caching [KGPB05] focuses on accelerating rendering of glossy materials, by caching an optimized representation of the radiance received on a surface. This method enables view-dependant reflections to be rendered correctly.

Biased algorithms have evolved and recent research has attempted to use machine learning techniques to accelerate rendering of GI effects. The *Deep Illumination* [TF17] approach uses a GAN to translate diffuse albedos, normals and depth maps to a global illumination component layer, and obtained good success at predicting indirect illumination in real time for diffuse materials. The network requires specific training for each scene to be rendered, but is able to extrapolate and adapt to dynamic objects and new shapes introduced.

To overcome the limitations of diffuse-only materials of current machine learning renderers, and to make the renderer easily usable without the need of offline training, we attempt a more general approach to resolving GI based on the estimation and caching of radiance maps for indirect illumination only, by combining Radiance Caching and a neural network that reconstructs and denoises radiance maps. Indirect lighting is the primary cause of strong noise in Monte Carlo rendering, and is much more difficult to clear than first bounce lighting due to the high dimensionality of the paths. Rendering can therefore be accelerated by predicting approximate but noise-free radiance maps that can be interpolated and used to obtain the indirect illumination component of the final image. Thanks to the slowly changing nature of indirect illumination, artifacts and bias are not very visible in the general case, while the overall predicted GI looks convincing and noise-free.

In contrast to full image level methods, OSR uses Path tracing to find the first intersection in the scene, where a Convolutional Autoencoder predicts a high quality, geometry dependant radiance map from a path traced map rendered at just 1 sample per pixel (**one-shot** map), a depth and a normals map. Using the high quality radiance maps we can approximate all indirect illumination contributed from Path tracing bounces beyond the first one. We use a neural network to predict high quality radiance maps to accelerate rendering of GI effects. Our approach works with a wide range of material types, and does not require any offline pre-computation or per-scene training.

2. Related Work

Recent projects have used Machine Learning for rendering purposes. We present some of the most relevant to our context.

The most immediate way to apply Machine Learning to graphics and ray tracing is to operate on the final rendered image level. These approaches take as input a scene rendered from the final camera's viewpoint, and attempt to output a transformation that results in higher visual quality, removal of noise, or addition of effects.

One of the first machine learning based approaches to improve rendering quality [KBS15] used a neural network to obtain filter parameters to de-noise path traced images. The method relies on

collecting primary features such as world coordinates, surface normals, texture values and illumination visibility from a ray tracer, from which secondary features are computed: gradients, mean and deviation. A Multi Layer Perceptron (MLP) uses the secondary features to output filter parameters. The method achieves good denoising quality, but requires the use of a modified ray tracer based on PBRTv2 [PH10]. *Kernel-predicting convolutional networks for denoising monte carlo renderings* [BVM*17] and the recent extension *Denoising with Kernel Prediction and Asymmetric Loss Functions* [VRM*18] improve denoising networks by separating the processing of diffuse and specular layers with Convolutional Neural Networks (CNN). This approach is also highly applicable to existing ray tracers, as many can natively output separate layers for diffuse, specular, Z-buffer, mist and others. The separation of layers allows the network to better handle the high dynamic range of input values, and the introduction of logarithmic transforms to the input data further increases performance. The CNN shows excellent performance with moderate noise.

A method proposed by Chaitanya et al [CKS*17] differs from the other examples as it does not take inputs with a small number of samples per pixel, but with exactly one sample. By retaining information from previous frames in an animation, the Convolutional Autoencoder is capable of reconstructing missing details given a very small amount of information. This method is particularly suited for fast, interactive animations previews. The above approaches are advanced denoising systems, and cannot create information that was not captured by the rendering engine or missing due to the low quality of the output. We highlight some past research that focused on adding Indirect Illumination and Global Illumination effects using neural networks by operating on the image plane level in the following.

A CNN implementation *Deep Shading* [NAM*17] predicts screen-space effects such as Ambient Occlusion, Motion Blur, Anti-Aliasing and Diffuse Indirect Illumination. The CNN takes OpenGL rasterization primary features, and produces outputs that can match real-time algorithms typically used in video games, while being able to generate any combination of effects in a single pass. While this approach does not attempt to achieve photorealistic results, a Conditional Generative Adversarial Network (CGAN) in *Deep Illumination* [TF17] is trained on specific scenes, with diffuse surfaces, to generate realistic and accurate GI effects. Despite being trained on specific scenes, the network is able to deal with moving objects and new shapes introduced. Its temporal stability makes it suitable for producing animations.

Global illumination with radiance regression functions [RWG*13] focuses on realtime indirect illumination rendering using a neural network that learns the relationship between local and contextual attributes such as vertices and light position, to the indirect illumination value. This method shows very good performance and quality, although it is limited to point light sources and requires pre-baking of the Radiance Regression Function for each scene.

A different approach is to accelerate convergence of existing Path tracers and Bidirectional path tracers. Reinforcement Learning (RL) [DK16] exploits the similarity between the Rendering Equation and Reinforcement Learning. The 3D scene is subdivided

into Voronoi cells, each with an importance map dome that is updated using Reinforcement Learning to remember the most efficient light path directions. The system is a path tracer that learns to dynamically update local importance sampling maps to increase its path efficiency and to reduce the number of zero-contribution paths. A similar idea is present in *Machine Learning and Integral Equations* [DK17], where an approximate solution to the integral equation is learned. *On-line Learning of Parametric Mixture Models for Light Transport Simulation* [VKŠ*14] optimizes learning of difficult sampling distributions to guide standard ray tracing algorithms, significantly improving the importance accuracy of light rays.

Deep Scattering [KMM*17] shows the power of Neural Networks when applied to a very specific use case: rendering of clouds. This method is able to achieve extremely high quality in the generation of complex lighting effects such as cloud silverlining by using a hierarchical 3D representation of the cloud structure.

3. Contribution

We propose One-Shot Radiance (OSR), a new rendering method that separates the processing of direct and indirect lighting. OSR is able to produce convincing indirect illumination, including glossy reflections and ambient occlusion, without any preprocessing on the scene. Our main contributions are:

- Use of a Convolutional Autoencoder to predict high quality radiance maps from low quality data for indirect illumination;
- Reintegration of direct illumination using a separate integrator;
- Progressive sampling and smooth interpolation of indirect illumination values without pre-computation and additional storage.

4. Method

One Shot Radiance renders the final image by computing direct and indirect illumination independently. The direct illumination pass uses a standard ray tracer with depth fixed at 1. The indirect illumination subdivides the image into tiles, and computes several radiance maps within the tile. Each radiance map is obtained by ray tracing a low resolution intensity, depth and normals map from the first intersection point into the scene, augmented by the Convolutional Autoencoder. The radiance maps are used to compute the final indirect illumination contribution of the pixels.

4.1. Illumination components

OSR splits rendering of direct illumination and indirect illumination. The indirect illumination component evaluates cached radiance maps, obtained efficiently using a deep neural network that reads local geometrical information of the scene. A standard Path tracer evaluates the Rendering Equation [Kaj98] recursively:

$$L_o(x, \vec{\omega}_0) = L_e(x, \vec{\omega}_0) + \int_{\Omega_{4\pi}} f_r(x, \vec{\omega}_0, \vec{\omega}_i) \cos(\theta_i) L_i(x, \vec{\omega}_i) d\omega_i. \quad (1)$$

L_e is the radiance emitted by the surface, f_r is the BRDF or BSDF of the material, the \cos term is used to compute the irradiance accounting for the incident angle of the incoming radiance L_i from the next bounce. A ray in Path tracing bounces on surfaces in the scene until a light is hit, or the path is terminated. The recursively evaluated radiance, the BRDF f of the material and the

viewing direction $\vec{\omega}_i$ are used to obtain the final pixel value. OSR approximates the evaluation of the Rendering Equation by collapsing all the light bounces beyond the first in a single step. The ray tracer shoots a ray to find the first intersection point, and evaluates on its hemisphere a One-Shot radiance map, a depth map, and a normals map. These three images are the inputs of our Convolutional Autoencoder, which returns a higher quality radiance map. Previous research has achieved excellent degrees of success in denoising and reconstructing missing parts of the image from the output of a path tracer using Convolutional Neural Networks. This kind of network is particularly suited at extracting high level information from the locality of the image data. In the context of OSR, we chose to implement a Convolutional Autoencoder, as the noisy input can be associated to a highly lossy and compressed version of the same image when rendered at a higher number of samples per pixel. The output radiance map is placed back on the hemisphere around the first intersection point, and contains an approximation of all the recursive indirect radiance that Path tracing would evaluate over time. The Rendering Equation therefore becomes

$$L_o(x, \vec{\omega}_0) = L_e(x, \vec{\omega}_0) + \int_{\Omega_{4\pi}} f_r(x, \vec{\omega}_0, \vec{\omega}_i) \cos(\theta_i) R_i(\vec{\omega}_i) d\omega_i + \sum_{l \in \text{lights}} f_r(x, \vec{\omega}_0, \vec{\omega}_l) \cos(\theta_l) L_e(l, \vec{\omega}_l) V(x, l) \quad (2)$$

We replaced the recursive radiance term with R , the high quality radiance map obtained from the neural network, and evaluate it in the same way according to the BRDF f of the surface and the viewing direction $\vec{\omega}_i$. V is the visibility term of the direct illumination component for each light source.

Evaluating the entire Radiance map R would still be expensive. Our implementation uses Multiple Importance Sampling [VG95] with a small fixed number of samples to obtain indirect illumination values. We alternate sampling from R as if it were an environment map with perfect visibility, and from the probability distribution of the BRDF. Ambient occlusion is encoded into these local environment maps because they are taken from the point of the of the intersection point. This environment map does not contain the direct contribution of light sources, which is added back to the final image via a separate direct illumination pass.

To include direct illumination, the first intersection point also generates shadow rays to light sources (not shown in the figure). It is important to exclude direct light information from the Radiance maps, as they do not have a resolution high enough to produce accurate shadows.

4.2. Progressive refinement and interpolation

Instead of evaluating a Radiance map at each pixel of the image, OSR accelerates the rendering process by sampling a few pixels, interpolating their indirect illumination values, and progressively refining the final picture by adding samples. Sampling and interpolation only applies to indirect illumination, the direct illumination passes are performed over all pixels.

The interpolation method of OSR does not use any precomputation to determine the best sampling locations. We compute a grid of sampling points on the image plane, evaluate a radiance map at

each point, and interpolate all other values. After each complete pass on the image, the distance between points on the grid is reduced by a constant factor, allowing the algorithm to progressively refine the resolution of the indirect illumination component.

The interpolation strategy for points that are not sampled is based on both the distance from the sampled radiance maps and the surface normal at the primary intersection. The primary intersection is the closest non-specular intersection point of a ray shot from the camera. If a ray hits a transmission or mirror material, we follow the bounce recursively, and place the primary intersection point when the bounced ray hits again. The weight of each radiance map for pixel i is:

$$w = w_p \cdot w_n + w_p + \epsilon \quad (3)$$

Where the position weight w_p is:

$$w_p = \text{dist}(p_i, p) / r \quad (4)$$

$\text{dist}(p_i, p)$ measures the distance in pixels on the image plane between the pixel being evaluated and the cached radiance map, and r is the distance between two points in the grid.

The normals weight w_n is maximal when the pixel's intersection point and the cached radiance map's normals (n and n_i respectively) point in the same direction, and becomes zero when their dot product is negative:

$$w_n = 1 - \max\left(0, \left(\frac{n_i}{|n_i|} \cdot \frac{n}{|n|}\right)\right) \quad (5)$$

The weights w of the radiance maps are normalized and converted into sampling probabilities for the radiance sampling.

4.3. Neural Network

The Neural Network is one of the core components of OSR. The objective of the network is to predict a smooth and accurate radiance map from primary features that can be computed quickly by a raytracer.

Each input or output layer has 32×32 floating point values. The input is composed of 7 layers: One-shot (RGB), normals (XYZ), and distance (Z). The output has 3 layers: Radiance (RGB). Figure 2 shows an example set of input and output maps.

The maps are in hemispherical latitude-longitude equirectangular projection. The coverage of a hemispherical map is not the full sphere, but only the upper hemisphere visible from a scene intersection point, with the surface normal aligned towards the Z direction of the latitude-longitude map. The up vector used in the hemispherical maps is the same as the one specified in the global scene, and it is rotated by 90 degrees towards the global Y vector only when the surface normal also points towards Z. In our final model we use the L1 loss: $L1 = \sum_{i=0}^n |y_i - h(x_i)|$.

Where y_i is a ground truth data point, and $h(x_i)$ is a predicted value.

Our network architecture is shown in Figure 3 and is similar to the U-Net architecture [RFB15], a convolutional autoencoder with skip connections and regular dimensionality progression. The encoder and decoder have symmetrical structure: each encoder stage uses two 3×3 convolutions and doubles the dimensional depth,

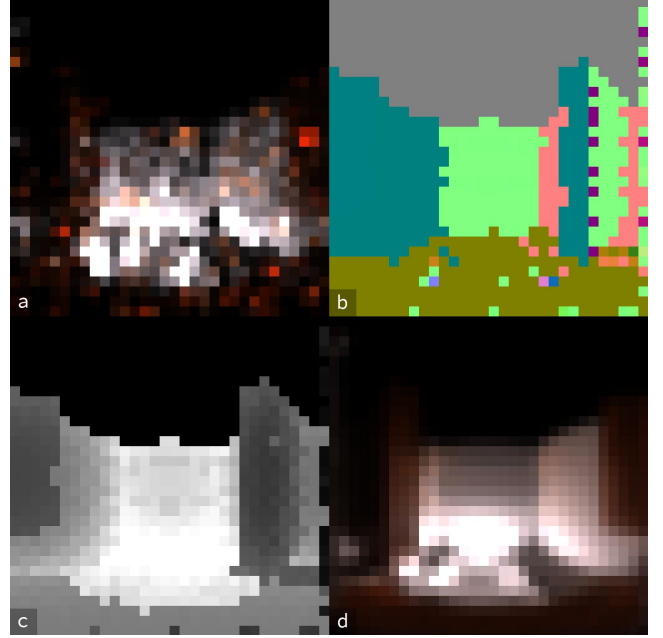


Figure 2: Examples of latitude-longitude hemispherical maps generated by OSR. This sample was generated from one intersection in the scene *bathroom*, part of the PBRTv3 example scenes [PJH18]. Image (a) is a path traced intensity map at 1 sample/pixel. Image (b) is a normals map. Image (c) is the distance map. Image (d) is the same intensity map, traced at 4096 samples/pixel, used as reference ground truth during training.

while each decoder stage has two 3×3 deconvolutions and reduces the depth by half.

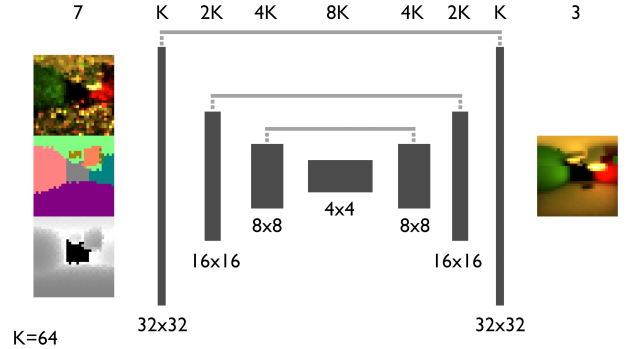


Figure 3: Network layout

All intermediate stages use batch normalization and LeakyReLU activation functions. The output stage has two 3×3 deconvolutions with LeakyReLU, and a final 1×1 convolution with ReLU activation to output the final data. Each downsampling stage uses a 2×2 Max Pooling, and the upsampling stages use 2×2 Bilinear Upsampling. We do not use any Dropout layer.

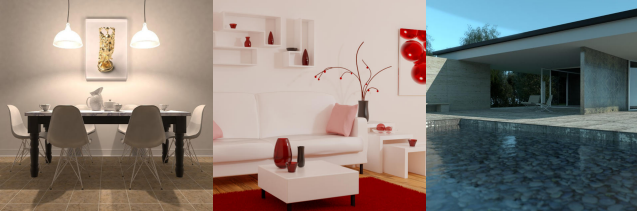


Figure 4: Some scenes from the training set (cropped to fit)

5. Implementation

Model training: A set of 43 scenes have been selected from the PBRTv3 example scenes[†], Benedikt Bitterli’s resources [Bit18], and our own custom created scenes. A subset of the scenes is shown in Figure 4. As OSR focuses on rendering indirect illumination, the selection of the training scenes have been weighted to include mostly interior scenes with difficult illumination, and scenes with strong global illumination.

Each of the scenes have been processed to generate a set of hemispherical maps. Similarly to the approach taken by Kalantari [KBS15], we change sampling algorithms and seeds to prevent the network from overfitting to specific noise patterns rather than higher level features: we use multiple samplers, including Sobol and Random, to produce varied noise patterns. We collected 16000 individual training examples. This dataset was sufficient in our tests to achieve good training results.

We implemented the neural network model and training process in Python using Pytorch (<http://pytorch.org/>). All machine learning processing has been conducted on a single machine with an Intel i7 4770 processor, 16GB of memory, and an Nvidia GTX 1060 6GB card for GPU acceleration.

We chose a base layer size of $K=64$, and a minimum hidden layer dimension of 4×4 . These parameters result in 3 downsizing steps and 3 corresponding upsampling steps.

We used the Adam optimizer included in PyTorch, with a learning rate of $6e-5$. We achieved good network performance after 20 minutes of training with mini-batches containing 32 examples each. Our training covers 3 epochs over the augmented dataset: more than half a million individual examples.

Our full dataset weights 0.5GBytes gzipped, and can be easily loaded into the memory of a single GPU when uncompressed. This helps us achieve high training performance. The trained model weights 20MBytes, and is small enough to be efficiently evaluated by both CPUs and GPUs.

We implemented data augmentation in our Pytorch data loader to include all combinations of rotation and flipping.

PBRT Extension: The OSR method and algorithm has been implemented by modifying PBRTv3 [PJH16], a C++ ray tracer implementing many popular algorithms.

Starting from PBRTv3, we implement a new `integrator` which evaluates direct and indirect illumination separately, and

communicates to the neural network to obtain the radiance map predictions. PBRT-OSR can operate in two different modes: *Reference* and *Rendering*.

While the *Rendering* mode can be used by the final user to render a scene, the *Reference* mode computes training examples given a scene. The *Reference* mode automatically generates a large number of examples suitable for both training and validation purposes. The number of tiles can be defined and determines the way the rendered image is subdivided into a regular grid. Each intersection in the grid is used to shoot a single camera ray into the scene, and the intersection found becomes the viewpoint of one set of examples. The high quality Path tracing render’s number of samples can be specified by the user. In the rendering process we use two independent steps to compute indirect illumination and direct illumination.

The direct illumination pass is handled using a standard *Direct Illumination* integrator implemented in the original PBRT software. The indirect illumination uses the *Path* integrator to collect the neural network’s input maps. The machine learning evaluation runs in a separate Python process running Pytorch. Each rendering thread has its own child process, and communication is handled through standard Unix pipes. Each Python evaluation process loads the saved model parameters, and reads flattened input data from `stdin`. The predicted output is written back to `stdout`.

6. Evaluation and Results

OSR is evaluated in terms of its network performance, final image quality, and performance. We analyze the output of the Convolutional Autoencoder in Section 6.1, perform an ablation study in Section 6.2 and evaluate image quality using established metrics like PSNR and Entropy in Section 6.3.

6.1. Neural Network Evaluation

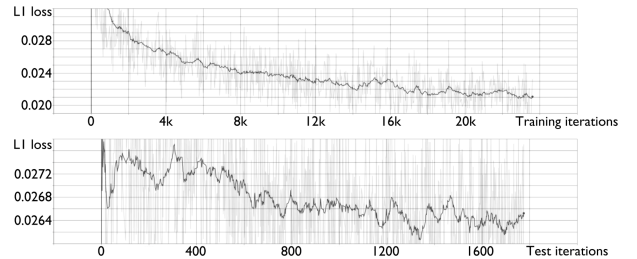


Figure 5: Training and Test L1 Loss in Model 11

Figure 5 shows training and test loss values during training. Our model reaches stable loss values over a 20 minutes learning period, without overfitting to the training dataset.

The network was trained on a collection of 3D scenes, and the evaluation is conducted on three selected scenes that were never part of the training dataset: *White Room Daytime* part of the original PBRTv3 example scenes [PJH18], *Veach Ajar* by Veach and adapted by B. Bitterli [Bit18], and *Mbed1*, custom created for the purpose of this evaluation.

The difference in amount and depth of indirect illumination paths across the test scenes allows us to verify that our network is able

[†] <http://pbrt.org/scenes-v3.html>

to deal with different input data quality seamlessly, and that it is able to extrapolate and adapt to geometry not encountered during training.

As with the training set generation, we obtain input maps and ground truth path traced radiance maps for several viewpoints located at primary surface intersection points. While the PBRT-OSR implementation re-normalizes the output images to match the expected intensity level of the entire radiance map, in our tests we compare directly using the final intensities obtained after the up-stream processing to provide an unbiased view of the network performance.

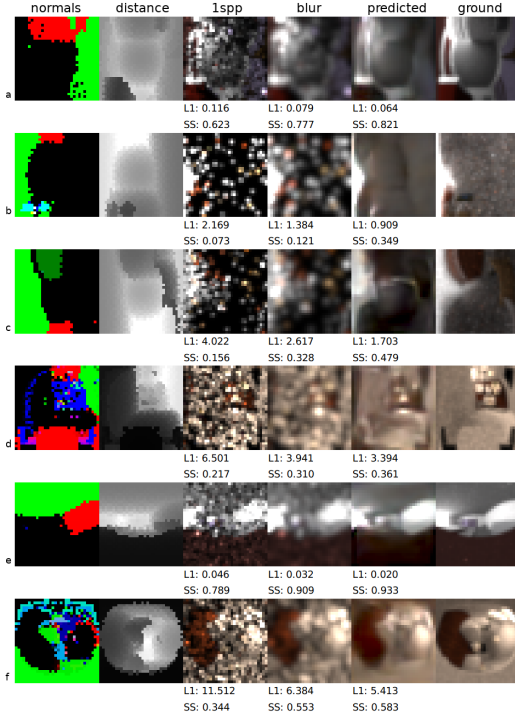


Figure 6: A random selection from the test scenes *Veach Ajar*, *Custom Mbed*, *White Room Daytime*. All examples show excellent noise removal when comparing *1spp* to *predicted*, with the predictions occasionally presenting less noise than the reference ground truth. In a) there is some color inaccuracy, with the predicted image’s purple area on the lower right corner being less saturated than the ground truth. b) and c), part of *Veach Ajar*, are very difficult due to the very sparse sampling of the input intensity map. They show excellent noise removal, producing less noise than the ground truth, although c) shows some shape distortions. d) and f) are less sharp than the ground truth, but still considerably more usable than the Gaussian blur versions.

Figure 6 shows a random selection of radiance maps predicted using our neural network model. The first three columns show the inputs of the network, and the result is compared to a simple Gaussian blur and a reference path traced ground truth rendered at 1024 samples per pixel. As many of the One-Shot path tracer outputs

comprise mostly of black pixels and a few very bright ones, standard image denoising filters such as Bilateral and Median Filter do not perform well. The Gaussian blur, although yielding softer outputs, is more capable at filling the black gaps.

The Gaussian blur uses a one standard deviation filter width, chosen for its good compromise between smoothing power and blurriness. A smaller radius would not be able to remove much noise, while a larger radius would yield considerably blurrier results compared to either ground truth or network predicted output. Due to the very sparse samples generated by the path tracer, a simple Gaussian blur is a significant improvement over the 1spp (1 sample per pixel) intensity map.

The examples show that the network predicted output can consistently outperform the Gaussian blur by producing sharper images, preserving more detail, and removing more noise. We can observe that:

- The predicted result is generally sharper than the Gaussian blur. This confirms the fact that we would not be able to use a larger radius for the Gaussian blur for difficult cases without losing even more details.
- The network is able to reconstruct some details that are missing from the 1spp intensity map, although it can cause artifacts.
- The network has effectively learned to use adaptive blurring filters. In simple cases it behaves very similarly to a planar Gaussian blur, but in the general case it is able to adapt to different sampling densities more effectively.
- The network eliminates all visible noise, and can produce images that look smoother and with less noise even when compared to the high quality path traced reference images. This shows the ability of the network to extrapolate from the training dataset, which still contains a small amount of noise in its ground truth examples.

To verify our claims, we run metrics on a large number of radiance evaluation points collected from the testing scenes, totalling over 1000 distinct testing examples that were not seen during training. For each example set of images, we compute the L1 absolute difference between predicted and reference images:

$$L1 = \frac{1}{n} \sum_{i=0}^n |p_i - g_i| \quad (6)$$

p_i is a predicted pixel value, g_i is a reference pixel value. Figure 7 shows L1 and Structural Similarity Index [WBSS04]. The Gaussian blur does considerably increase the quality of the radiance maps compared to using raw 1spp renders. The structural similarity increases, as the blur fills many of the black gaps present in the path traced map.

The network output considerably outperforms the Gaussian blur in both L1 and structural similarity metrics. We confirm that for both metrics the samples belong to different probability distributions by computing the Kruskal-Wallis null hypothesis testing [KW52] p values for L1 and Structural Similarity. We verified the p values to be less than 0.00001.

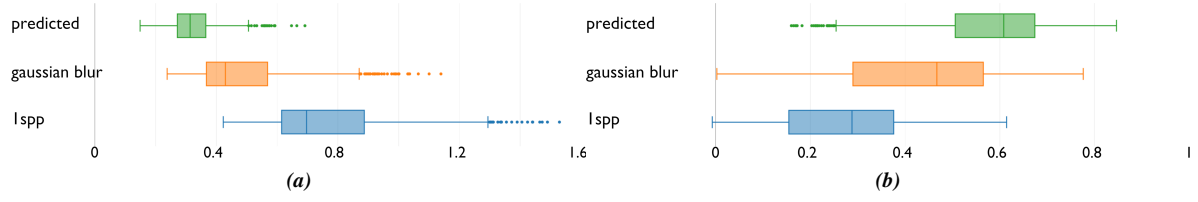


Figure 7: (a) L1 absolute difference, (b) Structural Similarity

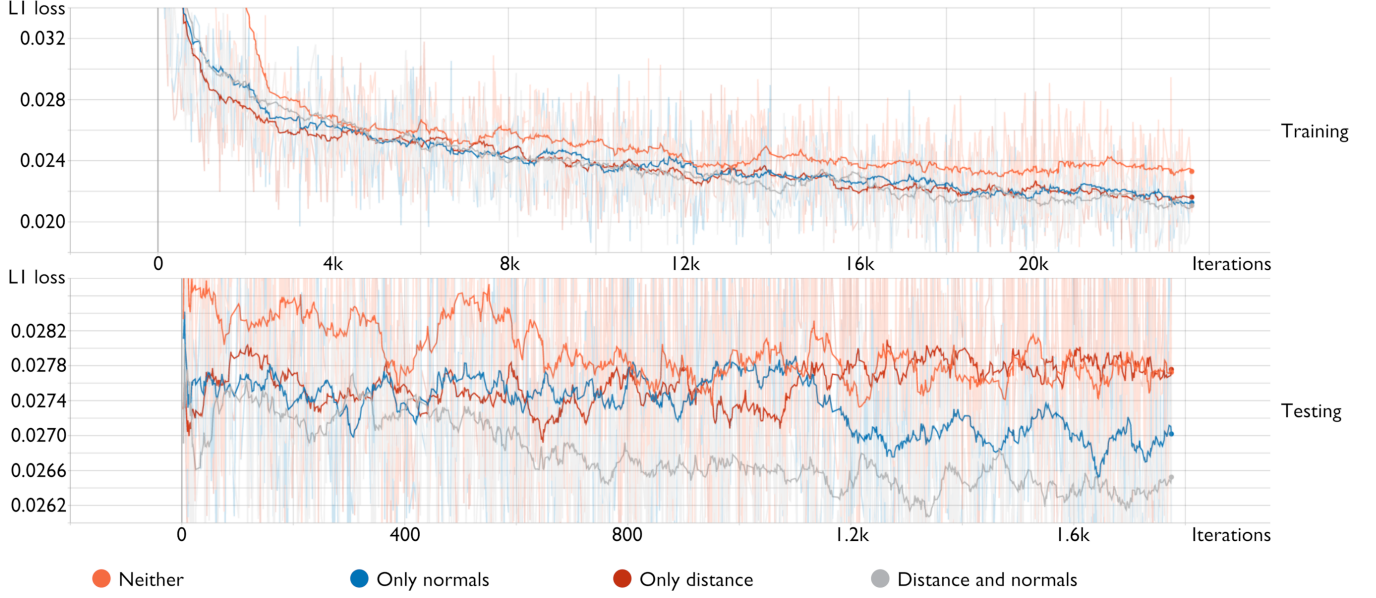


Figure 8: Training loss ablation testing. Removing information from the input data slows down convergence of the loss values. The effect is visible on the training set, but becomes more evident on the test set.

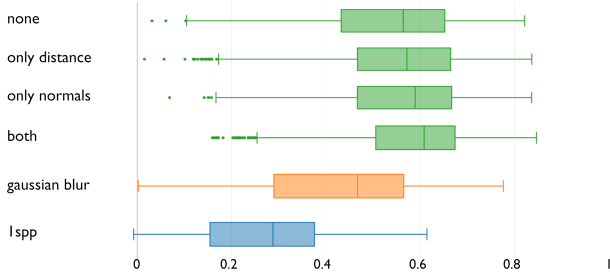


Figure 9: The box plots show structural similarity values in our ablation testing. *None*: predicted results with the network trained on intensity maps only. *Only distance*: network trained with intensity and distance maps. *Only normals*: network trained with intensity and normal maps. *Both*: network trained with intensity, distance and normal maps. *Gaussian blur*: Gaussian blur applied to the input intensity map. *1spp*: input intensity map path traced at 1 sample per pixel.

6.2. Neural Network Ablation Study

The ablation study aims to verify hypotheses about the data that the neural network uses to produce accurate predictions. Training is conducted using the entire dataset of intensity, normals, and distance maps, and repeated with the normals, distance, or both components removed from the network’s inputs. The structure of the network is left unchanged, and the ablation is implemented by setting the target components to be zero arrays. The evaluation mode is conducted in a similar way, by setting the ablated channels to zero arrays.

Figure 8 shows loss values during training and testing using the four different configurations. The use of only One-shot maps performs better than a simple blur, but is improved by the use of normal maps. Using distances without normals does not yield better performance, but the combination of all three inputs significantly outperforms the other configurations in the test suite.

The Structural Similarity Index test on the entire test suite in Figure 9 confirms that the addition of normal or distance maps help the network predict more accurate results, with the normals being slightly more effective than distances alone. The combination of

both additional layers further increases accuracy, and in particular improves the lower quartile significantly.

6.3. Final rendering evaluation

The evaluation of the final images is based on both qualitative and quantitative metrics. We render each of our test scenes at different levels of quality, and present observations, statistics and comparisons.

We first analyze rendered images of the scene *White Room Daytime*. We use OSR and Path tracer integrators at increasing levels of quality in order to pick reasonable sampling levels for both algorithms for the comparison.

Figure 10 shows OSR and Path tracer plots of the scene rendered at different levels of quality. The Path tracer uses power of two sampling rates, from 1 to 1024 samples per pixel. A reference image is also generated using Path tracing at 2048 samples per pixel. OSR is not based on a per-pixel quality setting, but on two distinct settings: the number of samples per pixels for the direct illumination integrator, and the number of tasks to be processed in the indirect illumination pass. A *task* is a single computational job in the indirect illumination pass, that corresponds to a rectangular region of the rendered image. A task is responsible for collecting the input maps in the region, evaluating them through the neural network, and adding the final light contributions to the image film. OSR heuristically splits indirect illumination rendering into tasks to distribute the computational load onto multiple CPU cores. During these tests we choose a number of direct illumination samples to produce a low noise first-bounce component. We then render the scene at different indirect tasks number, from 0 (no indirect component at all) up to 512.

The plots for the Path tracer deliver the expected results: similarity with respect to the reference increases every time the number of samples is doubled, and the amount of noise decreases at a steady rate.

For OSR the similarity to the reference increases slowly until 16 tasks, after which it remains almost stationary. Even though the metric does not appear to change much, the output image does have differences. The similarity metric saturates at this level due to the fact that OSR is not an unbiased algorithm even if it is capable of infinite progressive refinements. Some differences in the image cannot be cleared with longer rendering time, and any artifacts need to be judged subjectively.

The amount of noise decreases very slightly after each increase in number of tasks, although it starts at a significantly lower level than Path tracing: with rendering times below 3 minutes, PSNR values for Path tracing are above 220dB, compared to the 210dB of OSR. The OSR indirect passes do not produce much visible noise, with the small amount present being generated mainly by the direct illumination component.

As quality does not increase significantly in OSR after a certain number of tasks, we select the 16 tasks rendering to perform subjective comparisons. This image took 75 seconds using OSR, and we compare it with the Path traced render with the closest rendering time (73 seconds at 32S/px), and the reference rendered at 2048S/px (4445 seconds).

Figure 11 shows a comparison between Direct Illumination only, OSR and Path tracing. The OSR output looks much less noisy than the equal time Path tracing: the image generated by a Path tracer given the same amount of rendering time. Lighting on the spherical lamp looks smooth despite a small amount of light bleeding from the windows area. The light bleeding is more severe in OSR near the windows, where the radiance maps were not sampled densely enough to achieve the required contrast to match the reference. Global illumination details in darker areas look very convincing and close to the reference.

It is important to point out that the noise still visible in the OSR output is not caused by our method, but by the re-integration of the direct illumination layer. This can be verified by observing that the noise patterns between the OSR image and the one produced by the Direct Illumination integrator are identical.

Glossy and Specular materials: One of the key properties of OSR is its ability to work with a wide range of materials, including glossy surfaces. GI reflections heavily depend on the quality of the radiance maps. The Neural Network evaluation (Section 6.1) showed that a Gaussian blur applied on the One Shot radiance maps offers a good level of similarity compared to the ground truth. Figure 12 shows a sphere with a highly glossy surface under difficult lighting conditions. The Direct Illumination integrator in Figure 12(a) is almost completely black, confirming that all reflections are indirect. Blurred radiance maps may be sufficient to handle materials with a low level of glossiness or on low importance scene objects. The Neural Network in OSR brings improvements in the rendering quality of shinier surfaces. For example, blurred radiance maps do not have sufficient resolution in the dark areas (compare Figure 12(c) and (d)) and the Neural Network produces more stable and detailed output so that reflected shapes are better preserved. In contrast to denoising and blur filters, OSR can further be tuned by increasing the size of the predicted radiance maps, which directly reduces resolution-induced blur in the final result. The computational overhead of (d) compared to (c) is 40%, which can be improved in future extensions by adaptively choosing a radiance map enhancement strategy depending on the material properties.

Specular highlights, reflections and transmission materials are handled by following the original ray, and evaluating the radiance maps after the bounce. The threshold between the first and secondary ray bounce in OSR has therefore slightly different semantics from most ray tracers as perfect mirrors and transmission ray do not increase the depth counter. These specular rays are also ignored in the depth count of the Direct Illumination pass of OSR to provide a correct complementary integrator. In the details of Bathroom Green by cenobi [Cen12] in Figure 13, the mirror and glossy highlights preserve the original level of detail. OSR brings a significant noise level advantage with a rendering time of 57 seconds, while the Path Tracer took 56 seconds.

Interpolation: Figure 14 shows two images rendered at a limited number of tasks. The simple interpolation strategy only linearly interpolates using pixel distances on the image plane. Light bleeding and hard artifacts are clearly visible on the objects. We resolve some major artifacts by including surface normals in the weighting system (Section 4.2). Some artifacts remain near the edges due

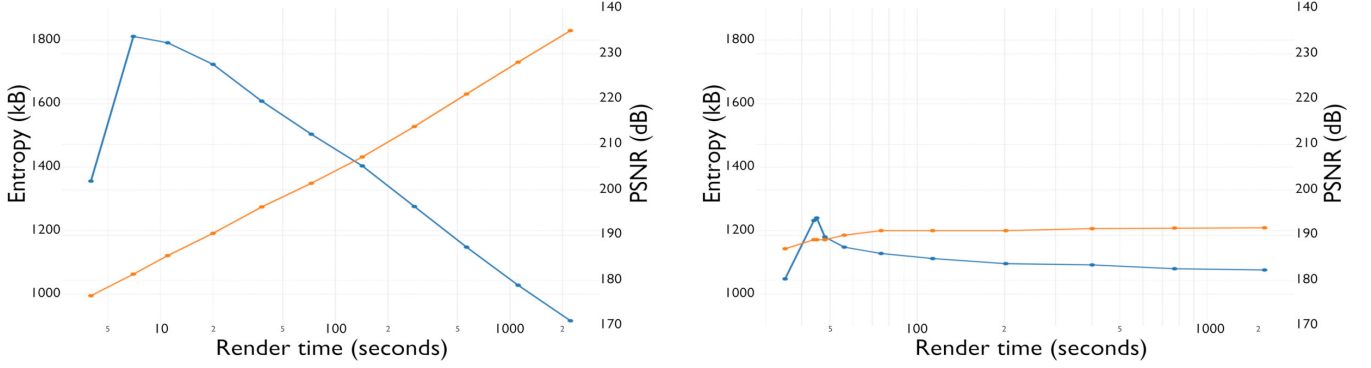


Figure 10: Quality and noise metrics on White Room Daytime. Left: OSR, Right: Path tracing. Render time: total rendering time in seconds. Entropy: indication of the amount of noise, measured as the final image size after PNG compression. PSNR: Peak Signal to Noise Ratio, a measure of the similarity between an image and a ground truth.

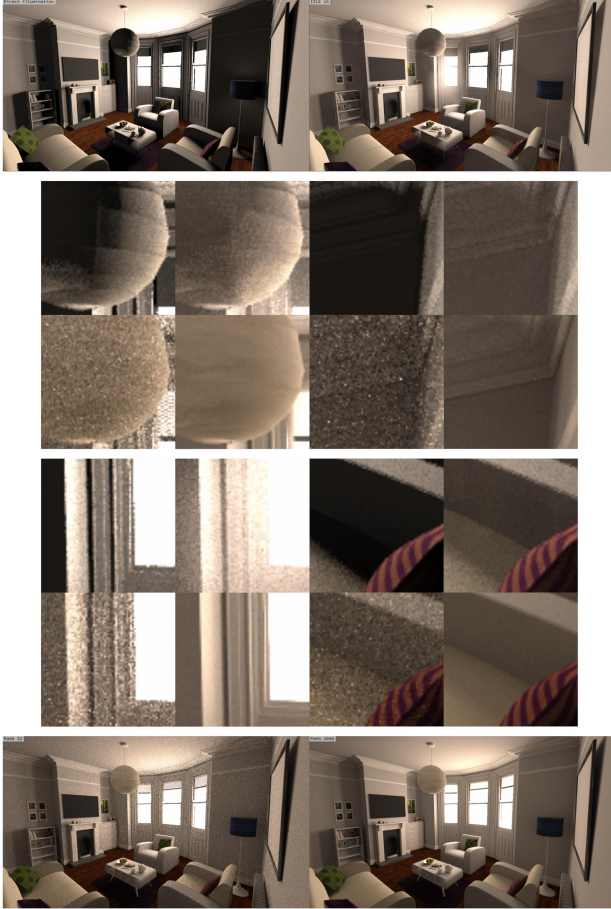


Figure 11: Comparison between Direct (top-left), OSR (top-right), Path 32 samples/pixel (bottom-left) and Path 2048 samples/pixel (bottom-right)

to the very low number of samples, while the overall image looks smooth.

Increasing the number of indirect illumination passes in OSR only affects computational time. Memory usage remains constant, as each interpolation pass is independent and does not require any data from previous passes.

7. Discussion

The OSR method offers a new biased rendering method for global illumination capable of producing high quality results efficiently, while supporting a wide range of material types and scene compositions.

Compared to other methods, OSR does not require any form of pre-computation on the target scene, and accelerates the computation of global illumination at a virtually unbounded number of indirect bounces at the cost of a small amount of bias introduced. The typical use scenario is rendering an interior 3D scene where indirect light is significant. Most interior scenes have strong indirect lighting, making light paths computationally intensive.

Faster estimation of indirect light through a neural network can drastically reduce the amount of noise present in the scene, and the typical low-frequency variation of indirect illumination easily masks away minor artifacts and interpolation imprecisions that originate from the machine learning subsystem. Thanks to the preservation of a standard direct illumination pass in the final image, most of the details and textures present in the scene are preserved in the final output.

OSR splits the processing of direct and indirect illumination, allowing the user to better tune the amount of computation to be used for each component

Limitations: Even though the progressive refinement algorithm permits the user to set an arbitrary number of passes, OSR remains a biased approach to global illumination. The neural network, although very accurate in typical scenarios, can produce artifacts, inaccurate results, and loss of detail, causing hard to correct errors.

A second important limiting factor is the fixed resolution of the

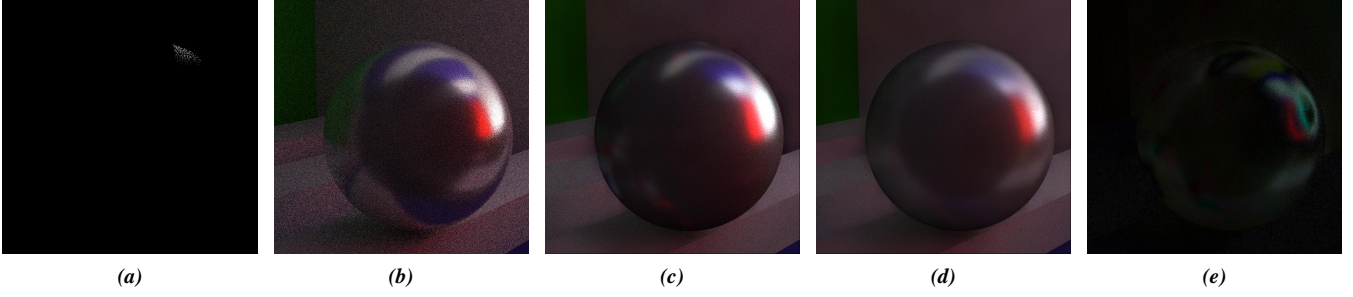


Figure 12: A direct comparison between (a) Direct illumination, (b) Path tracing, (c) OSR Gaussian blur, (d) OSR Neural Network, and (e) the difference between (c) and (d). The baseline method (c) misses several details on the lower left part of the sphere that have been correctly predicted in (d) when compared to (b).

radiance maps, set for OSR at a default of 32x32 pixels. Small details are inevitably lost.

These two limitations become particularly visible when computing globally illuminated glossy reflections, which appear less defined, although less noisy, than the path traced reference.

Temporal stability is another limitation of OSR. The rendering tiles can have large variations from one sample to another, and while being perceived as smooth transitions in a single frame, animations would display them as low frequency flickering of large areas in the scene. The lack of temporal stability indicates that OSR would not be adequate for animation rendering. To solve the temporal stability issue, a persistent caching system for radiance maps can be implemented, allowing animations to be rendered at faster

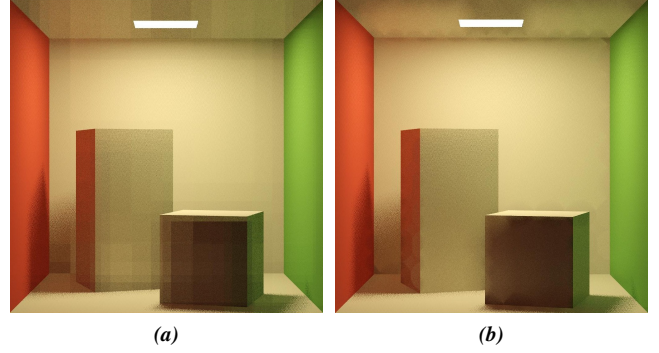


Figure 14: Comparison between simple distance based interpolation (a) and interpolation based on both distance and surface normals (b). Using surface normals improves smoothness across surfaces, and removes large artifacts and light bleeding on the edges of the cubes.

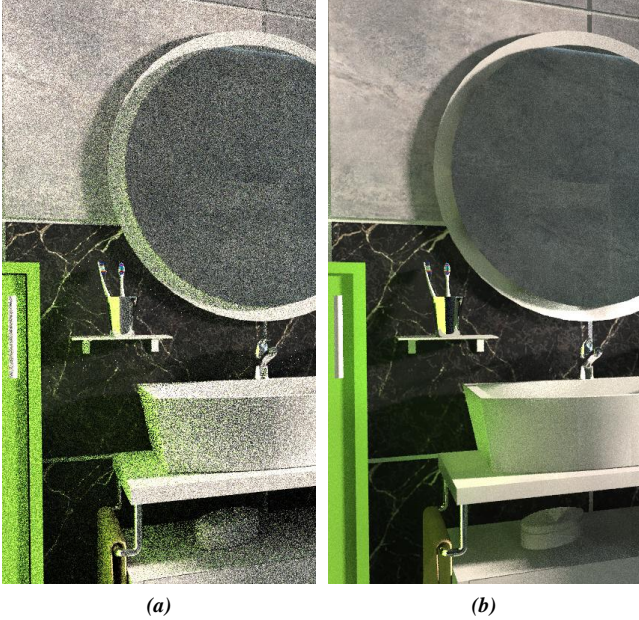


Figure 13: Crop of the scene Bathroom Green. (a) Path tracing, 56 seconds. (b) One Shot Radiance, 57 seconds.

rates and with less temporal noise caused by flickering of radiance maps. Due to the low resolution of the indirect radiance maps, OSR is not capable of producing accurate caustics, which require a much denser sampling of indirect light.

The progressive refinement algorithm used in OSR requires no preprocessing and very little additional memory to run. However in some scenarios predetermined and optimized radiance interpolation points can be a more effective solution, and implementing the possibility to choose between the two strategies would be a useful future extension.

8. Conclusion

We have presented *One-Shot Radiance*, a novel ray tracing method that uses Convolutional Autoencoders to obtain high performance and accurate global illumination effects. We show that our method achieves competitive performance on a CPU, while being able to produce higher quality images than same-time Path tracing, with a significantly smaller amount of noise. Our method supports a wide range of material types and does not need offline pre-computation

or per-scene training. If required, both, the used deep learning network and the Path tracing core map naturally to parallel hardware like GPUs, which has been shown to achieve real-time performance [PBD*10, GBCB16].

Resources: Website including plugin for Blender: <https://osr.jstudios.ovh/>. Source code repository: <https://github.com/giuliojiang/pbrt-v3-IILE>

9. Acknowledgements

This work has been kindly supported by Intel and Nvidia.

References

- [Bit18] BITTERLI B.: Rendering Resources. <https://benedikt-bitterli.me/resources/>, 2018. Accessed: 24/05/2018. 5
- [BVM*17] BAKO S., VOGELS T., MCWILLIAMS B., MEYER M., NOVÁK J., HARVILL A., SEN P., DE ROSE T., ROUSSELLE F.: Kernel-Predicting Convolutional Networks for Denoising Monte Carlo Renderings. In *Proceedings of ACM SIGGRAPH 2017* (2017), ACM. 2
- [Cen12] CENOBI U.: Bathroom Scene. <https://www.blendswap.com/blends/view/52486>, 2012. Accessed: 29/08/2018. 8
- [CKS*17] CHAITANYA C. R. A., KAPLAYAN A. S., SCHIED C., SALVI M., LEFOHN A., NOWROUZEZAHRAI D., AILA T.: Interactive Reconstruction of Monte Carlo Image Sequences Using a Recurrent Denoising Autoencoder. *ACM Trans. Graph.* 36, 4 (July 2017), 98:1–98:12. URL: <http://doi.acm.org/10.1145/3072959.3073601>, doi:10.1145/3072959.3073601. 2
- [DK16] DAHM K., KELLER A.: Learning light transport the reinforced way. In *International Conference on Monte Carlo and Quasi-Monte Carlo Methods in Scientific Computing* (2016), Springer Proceedings in Mathematics and Statistics Vol 241. 2
- [DK17] DAHM K., KELLER A.: Machine Learning and Integral Equations. *CoRR abs/1712.06115* (2017). URL: <http://arxiv.org/abs/1712.06115>, arXiv:1712.06115. 3
- [GBCB16] GOODFELLOW I., BENGIO Y., COURVILLE A., BENGIO Y.: *Deep learning*, vol. 1. MIT press Cambridge, 2016. 11
- [Kaj98] KAJIYA J. T.: *Seminal Graphics*. ACM, New York, NY, USA, 1998, ch. The Rendering Equation, pp. 157–164. URL: <http://doi.acm.org/10.1145/280811.280987>, doi:10.1145/280811.280987. 3
- [KBS15] KALANTARI N. K., BAKO S., SEN P.: A Machine Learning Approach for Filtering Monte Carlo Noise. *ACM Trans. Graph.* 34, 4 (July 2015), 122:1–122:12. URL: <http://doi.acm.org/10.1145/2766977>, doi:10.1145/2766977. 2, 5
- [Kel97] KELLER A.: Instant Radiosity. In *Proceedings of the 24th Annual Conference on Computer Graphics and Interactive Techniques* (New York, NY, USA, 1997), SIGGRAPH '97, ACM Press/Addison-Wesley Publishing Co., pp. 49–56. URL: <https://doi.org/10.1145/258734.258769>, doi:10.1145/258734.258769. 1
- [KGPB05] KRIVANEK J., GAUTRON P., PATTANAIK S., BOUATOUCH K.: Radiance caching for efficient global illumination computation. *IEEE Transactions on Visualization and Computer Graphics* 11, 5 (2005), 550–561. 2
- [KMM*17] KALLWEIT S., MÜLLER T., MCWILLIAMS B., GROSS M., NOVÁK J.: Deep scattering: Rendering atmospheric clouds with radiance-predicting neural networks. *ACM Transactions on Graphics (TOG)* 36, 6 (2017), 231. 3
- [KW52] KRUSKAL W. H., WALLIS W. A.: Use of ranks in one-criterion variance analysis. *Journal of the American statistical Association* 47, 260 (1952), 583–621. 6
- [LW93] LAFORTUNE E. P., WILLEMS Y.: Bi-directional path tracing. In *Compugraphics' 93*. 1993, pp. 145–153. 1
- [NAM*17] NALBACH O., ARABADZHIYSKA E., MEHTA D., SEIDEL H.-P., RITSCHER T.: Deep Shading: Convolutional Neural Networks for Screen-Space Shading. In *Computer Graphics Forum* (2017). 2
- [PBD*10] PARKER S. G., BIGLER J., DIETRICH A., FRIEDRICH H., HOBEROCK J., LUEBKE D., MCALLISTER D., MCGUIRE M., MORLEY K., ROBISON A., ET AL.: OptiX: a general purpose ray tracing engine. *ACM Transactions on Graphics (TOG)* 29, 4 (2010), 66. 11
- [PH10] PHARR M., HUMPHREYS G.: *Physically Based Rendering: From Theory To Implementation*. Morgan Kaufmann, 2nd edition, 2010. 2
- [PJH16] PHARR M., JAKOB W., HUMPHREYS G.: *Physically Based Rendering: From Theory To Implementation*. Morgan Kaufmann, 3rd edition, 2016. 5
- [PJH18] PHARR M., JAKOB W., HUMPHREYS G.: Scenes for pbrt-v3. <http://pbrt.org/scenes-v3.html>, 2018. Accessed: 25/04/2018. 1, 4, 5
- [RFB15] RONNEBERGER O., FISCHER P., BROX T.: U-Net: Convolutional networks for biomedical image segmentation. In *International Conference on Medical image computing and computer-assisted intervention* (2015), Springer, pp. 234–241. 4
- [RWG*13] REN P., WANG J., GONG M., LIN S., TONG X., GUO B.: Global illumination with radiance regression functions. *ACM Transactions on Graphics (TOG)* 32, 4 (2013), 130. 2
- [TF17] THOMAS M. M., FORBES A. G.: Deep Illumination: Approximating Dynamic Global Illumination with Generative Adversarial Network. In *arXiv preprint arXiv:1710.09834* (2017). 2
- [VG95] VEACH E., GUIBAS L.: Bidirectional estimators for light transport. In *Photorealistic Rendering Techniques*. Springer, 1995, pp. 145–167. 3
- [VG97] VEACH E., GUIBAS L. J.: Metropolis light transport. In *Proceedings of the 24th annual conference on Computer graphics and interactive techniques* (1997), ACM Press/Addison-Wesley Publishing Co., pp. 65–76. 1
- [VKŠ*14] VORBA J., KARLÍK O., ŠIK M., RITSCHER T., KŘIVÁNEK J.: On-line Learning of Parametric Mixture Models for Light Transport Simulation. *ACM Transactions on Graphics (Proceedings of SIGGRAPH 2014)* 33, 4 (aug 2014). 3
- [VRM*18] VOGELS T., ROUSSELLE F., MCWILLIAMS B., RÖTHLIN G., HARVILL A., ADLER D., MEYER M., NOVÁK J.: Denoising with Kernel Prediction and Asymmetric Loss Functions. *ACM Transactions on Graphics (Proceedings of SIGGRAPH 2018)* 37, 4 (2018), 124:1–124:15. doi:10.1145/3197517.3201388. 2
- [WBSS04] WANG Z., BOVIK A. C., SHEIKH H. R., SIMONCELLI E. P.: Image quality assessment: from error visibility to structural similarity. *IEEE Transactions on Image Processing* 13, 4 (2004), 600–612. 6